Journal of Neuroinflammation

RESEARCH

Open Access

Rebamipide (Mucosta®), a clinically approved drug, alleviates neuroinflammation and dopaminergic neurodegeneration in a Parkinson's disease model

Hye-Sun Lim[1], Jinyoung Park[2], Eunjeong Kim[3], Wonhwa Lee[4], Hwi-Yeol Yun[5,6,7], Seung Hoon Lee[8] and Gunhyuk Park[1*]

Abstract

Background Parkinson's disease (PD) is characterized by dopaminergic neuron loss, neuroinflammation, and motor dysfunction. PD is a multifactorial disease, with neuroinflammation driven by NLRP3 inflammasome activation representing an important component of its pathological progression. Therefore, we aimed to evaluate the therapeutic potential of rebamipide (Mucosta®), a clinically approved anti-inflammatory agent, in PD by targeting the NLRP3 inflammasome. Specifically, we examined the effects of rebamipide on neuroinflammation, dopaminergic neuron preservation, and motor deficits using BV2 microglia cells and a 1-methyl-4-phenyl-1, 2, 3, 6-tetrahydropyridine (MPTP)-induced mouse model.

Main body Rebamipide alleviated microglial activation and downstream neuroinflammation by suppressing the NLRP3–NEK7 interaction, resulting in dopaminergic neuron protection in the MPTP-induced PD model. Rebamipide downregulated IL-1β levels in BV2 microglia cells treated with α-synuclein and MPP^+. Molecular docking analysis revealed a high binding affinity between rebamipide and the NLRP3-NEK7 interaction interface. Surface plasmon resonance analysis confirmed the direct binding of rebamipide to NLRP3, with notable kinetic affinity, supporting its role as a novel NLRP3 inflammasome inhibitor. Rebamipide significantly downregulated IL-1β levels, microglial activation, and dopaminergic neuron loss in the MPTP mouse model by disrupting inflammasome activation. Rebamipide preserved dopamine levels in the striatum and improved motor deficits, including bradykinesia and motor coordination. The neuroprotective effects of rebamipide were neutralized in NLRP3 knockout mice, confirming the dependency of its action on NLRP3.

Conclusion Considering its established clinical use, this study supports repurposing rebamipide for treating PD and other NLRP3 inflammasome-driven neuroinflammatory diseases.

*Correspondence:
Gunhyuk Park
gpark@kiom.re.kr; parkgunhyuk@gmail.com
Full list of author information is available at the end of the article

Highlights

1. Rebamipide inhibited NLRP3 inflammasome activation in Parkinson's disease models.
2. Rebamipide reduceed neuroinflammation and protected dopaminergic neurons.
3. Rebamipide improved motor function by suppressing NLRP3-driven neurotoxicity.
4. Rebamipide represents a promising NLRP3-targeting therapy for Parkinson's disease.

Keywords Rebamipide, MPTP, NLRP3 inflammasome, Neuroinflammation, Parkinson's disease

Graphical Abstract

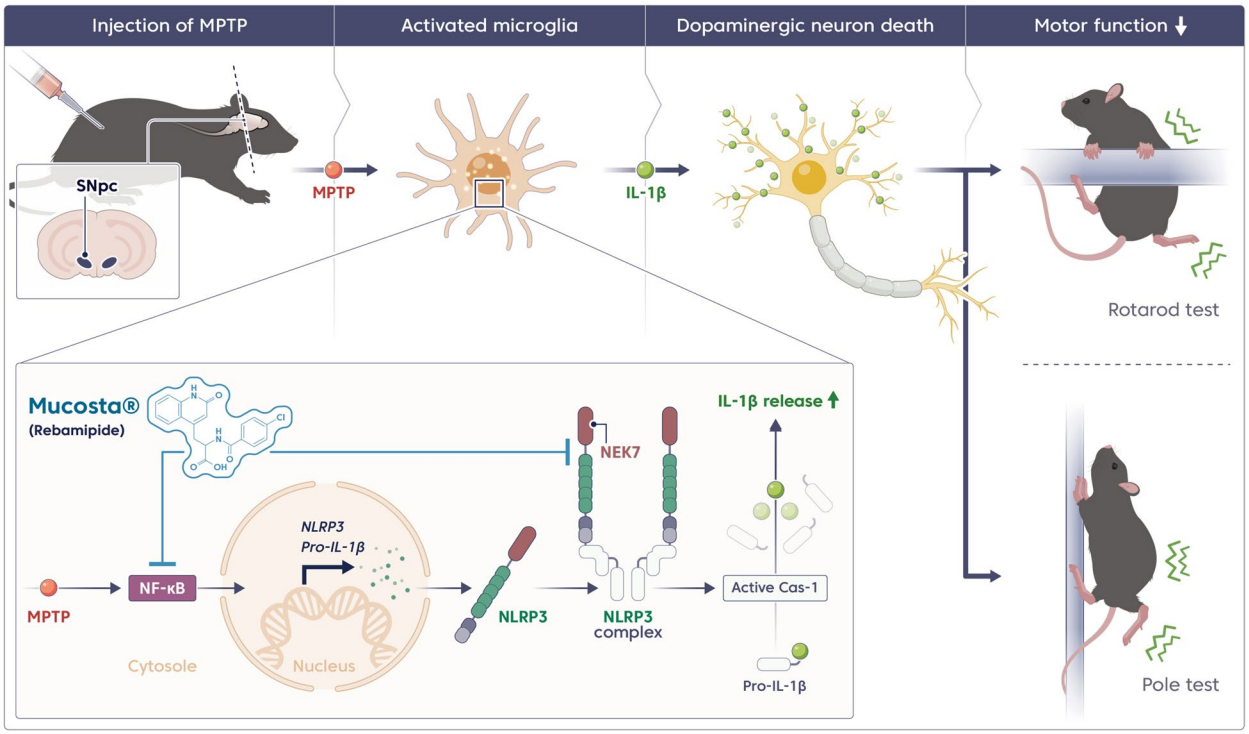

Background

Parkinson's disease (PD) is a common neurodegenerative disorder marked by progressive loss of dopaminergic neurons in the nigrostriatal pathway, resulting in dopamine deficiency and characteristic motor symptoms, including bradykinesia, tremor, and rigidity [1, 2]. A hallmark pathological feature of PD is the presence of Lewy bodies, which are intraneuronal inclusions primarily composed of aggregated α-synuclein [1, 2]. The precise mechanisms underlying dopaminergic neurodegeneration remain unclear; nevertheless, increasing evidence suggests the involvement of neuroinflammation, mitochondrial dysfunction, oxidative stress, and excitotoxicity [3, 4]. Among these, neuroinflammation has garnered attention as an important driver of disease progression. Elevated proinflammatory cytokines have been observed in patient tissues and animal models, particularly within dopaminergic regions such as the substantia nigra pars compacta (SNpc) [3, 4]. Activated microglia exacerbate neuronal loss by releasing neurotoxic mediators, thereby linking chronic inflammation to PD pathogenesis [3, 4]. Therefore, targeting microglia-mediated neuroinflammation has emerged as a promising therapeutic strategy for PD.

The NLRP3 inflammasome is a key regulator of innate immunity and has been increasingly recognized for its role in PD neuroinflammation [5]. Mechanistically, stimuli such as danger-associated molecular patterns (DAMPs) and pathogen-associated molecular patterns (PAMPs) simultaneously activate the NLRP3 inflammasome receptor, adaptor protein ASC, and caspase-1

(Casp1) [5]. Upon activation, the NLRP3 inflammasome triggers caspase-1-mediated cleavage of pro-IL-1β and pro-IL-18 into their mature forms, driving a potent inflammatory response [5]. This activation is facilitated by cellular mechanisms including ionic flux, reactive oxygen species (ROS) production, and lysosomal disruption [5–7]. NLRP3 inflammasome activation amplifies neuroinflammation and dopaminergic neuron loss in PD, rendering it a promising therapeutic target for interventions.

Rebamipide (Mucosta®; Fig. 1A), developed by Otsuka®, is a gastric mucoprotective drug widely used in Asia [8, 9]. Rebamipide stimulates prostaglandin synthesis, inhibits ROS generation, reduces inflammatory cytokine secretion, and attenuates neutrophil activation [10]. In addition to its gastrointestinal applications, rebamipide has been used to treat dry eye disease and has demonstrated efficacy in reducing ocular inflammation and improving corneal conditions [11, 12]. Importantly, rebamipide's anti-inflammatory effects have been demonstrated in other conditions, including bladder inflammation, collagen-induced arthritis, and inflammatory skin diseases via suppression of NF-κB signaling [13–17]. Emerging research on inflammasomes suggests the potential of rebamipide in inflammasome-driven diseases, such as gout [17]. Additionally, rebamipide shows neuroprotective properties in neurological disorders [18]. For example, rebamipide reduces Aβ production, suppresses intracellular Aβ oligomers, and improves cell viability by inducing cytoprotective genes [19]. Moreover, it stabilizes mitochondrial bioenergetics and enhances antioxidant activity, potentially mitigating 6-hydroxydopamine-induced PD [20]. Targeting the NLRP3–NEK7 interaction may be a promising approach to suppress inflammasome-driven neuroinflammation in PD. Despite

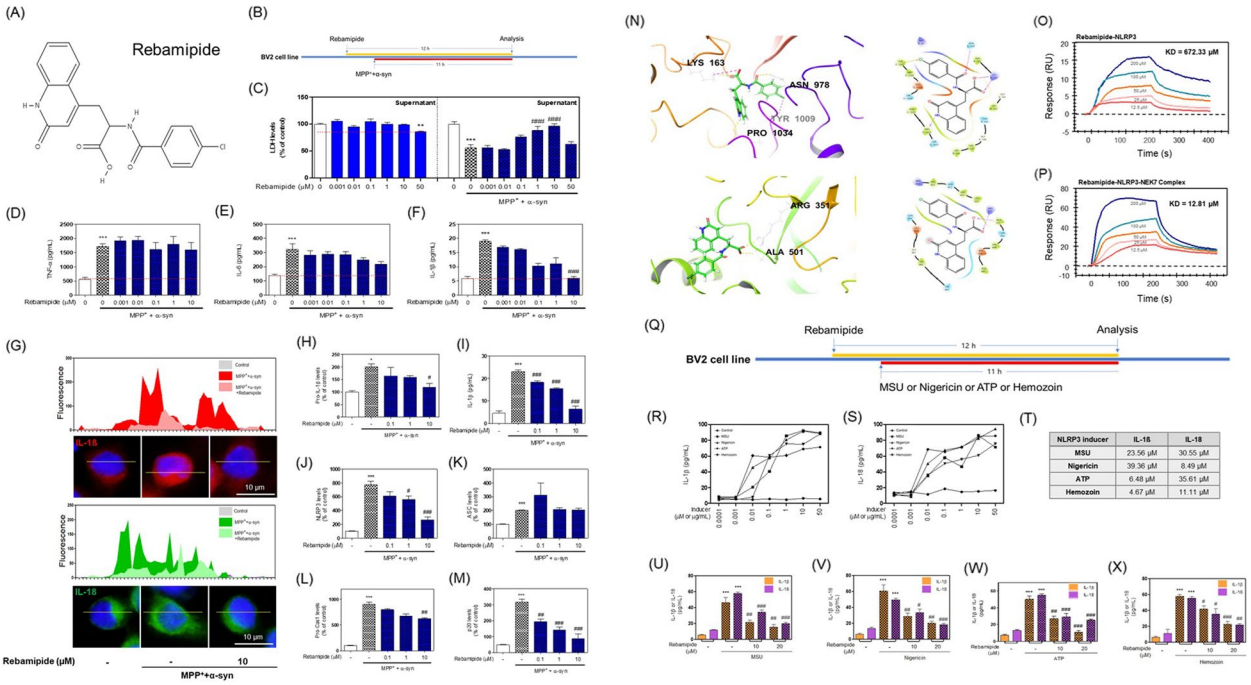

Fig. 1 Chemical structure of rebamipide. **A** Overview of the experimental design. **B** Protective effects of rebamipide on α-synuclein + MPP^+-induced cytotoxicity in BV2 microglia cells. **C** BV2 microglia cells were treated with rebamipide for 1 h and then stimulated with α-synuclein + MPP^+ for an additional 11 h. Lactate dehydrogenase (LDH) (**C**), TNF-α (**D**), IL-6 (**E**), IL-1ß (**F**, **G**, and **I**), pro-IL-1ß (**H**), and IL-18 (**G**) levels were evaluated. Inhibitory effects of rebamipide on NLRP3 (**J**), ASC (**K**), pro-caspase-1 (**L**), and p20 (**M**) in BV2 microglia cells were measured using ELISA. Molecular docking illustrating the binding interactions of rebamipide with the NLRP3-NEK7 complex and NLRP3 alone (**N**). The left panels depict 3D docking models, whereas the right panels represent 2D interaction diagrams highlighting key binding residues. Hydrogen bonds are indicated by purple arrows, halogen bonds by yellow arrows, and salt bridges by red and blue lines. Rebamipide interacts with ASN978, TYR1009, and PRO1034 of NLRP3 and LYS163 of NEK7, suggesting a role in disrupting the NLRP3-NEK7 interaction and modulating inflammasome activation. Surface plasmon resonance (SPR) sensorgrams demonstrating the real-time binding kinetics of rebamipide to NLRP3-NEK7 complex (**O**) and NLRP3 alone (**P**). Rebamipide exhibited dose-dependent binding, with a higher binding affinity for NLRP3-NEK7 complex than NLRP3 alone. Overview of the experimental design (**Q**). Inhibitory effects of rebamipide on NLRP3-induced upregulation of IL-1ß (**R**) and IL-18 (**S**) in BV2 microglia cells. BV2 microglia cells were treated with rebamipide for 1 h and then stimulated with MSU, nigericine, ATP, and hemozoin for an additional 11 h. IL-1ß and IL-18 levels were evaluated (**T**-**X**). Data are presented as mean ± standard error of mean (SEM). * $p < 0.05$, ** $p < 0.01$, *** $p < 0.001$, compared with the control group; # $p < 0.05$, ## $p < 0.01$, ### $p < 0.001$, compared with the α-synuclein + MPP^+ or NLRP3 inducers-treated groups

these findings, the precise mechanisms of rebamipide in PD, particularly its anti-inflammatory effects through NLRP3 inflammasome inhibition, remain unexplored. Therefore, we aimed to investigate the neuroprotective effects and mechanisms of rebamipide against 1-methyl-4-phenyl-1, 2, 3, 6-tetrahydropyridine (MPTP)-induced motor deficits and dopaminergic neuronal death, focusing on the NLRP3 inflammasome pathway.

Materials and methods

Chemicals

Paraformaldehyde (PFA), 3,3-diaminobenzidine (DAB), sodium chloride, sucrose, ethanol, histomount medium, dimethyl sulfoxide (DMSO), MPTP, hydrogen peroxide, phosphate-buffered saline (PBS), and sodium citrate buffer were purchased from Sigma–Aldrich (St. Louis, MO, USA). Biotinylated horse anti-goat antibody, goat anti-rabbit antibody, goat anti-mouse antibody, normal goat serum (NGS), normal donkey serum (NDS), and VECTASTAIN Elite ABC Kit were purchased from Vector Laboratories (Burlingame, CA, USA). Rabbit antityrosine hydroxylase (TH) antibodies were purchased from Millipore Bioscience Research (Bedford, MA, USA). Rabbit and mouse anti-Iba-1 antibodies were purchased from WAKO (Osaka, Japan). Rabbit anti-IL-1ß and IL-18 antibodies were purchased from Cell Signaling Technology (Beverly, MA). Enzyme-linked immunosorbent assay (ELISA) kits for IL-1ß were purchased from Abcam (Cambridge, MA). 1 Kb plus ladder and UltraPure™ DNase/RNase-Free Distilled Water were purchased from Invitrogen (Paisley, UK). ProNA Bandi-Green View for DNA and RNA stains were purchased from BD Translabs (Franklin Lakes, NJ). All other utilized reagents were of guaranteed or analytical grade.

BV2 microglia cell culture and treatments

Briefly, BV2 microglia cells (ABC-TC212S; AcceGen Biotechnology, USA) were maintained in Dulbecco's Modified Eagle medium (DMEM) supplemented with 10% heat-inactivated fetal bovine serum and 1% penicillin/streptomycin at 37 °C under 95% air and 5% CO2. BV2 microglia cells were treated with rebamipide (0.001–10 μM) for 12 h, followed by stimulation with α-synuclein and MPP^+ for 11 h. BV2 cells were incubated with rebamipide (0.001–10 μM) for 12 h and then stimulated with the NLRP3 inflammasome inducer (MSU), nigericin, ATP, or hemozoin for 11 h to establish the NLRP3 inflammasome inducer models. On the other hand, BV2 cells were incubated with rebamipide (10 μM) for 12 h and then stimulated with the NLRP3 inflammasome inhibitor (MCC950) for 11 h to establish the NLRP3 inflammasome inhibitor models. The experimental design timeline is shown in Figs. 1B, Q, and 4D.

LDH level measurements

Intracellular LDH levels were measured using a CytoScan™ LDH-cytotoxicity assay kit, according to the manufacturer's instructions. The absorbance was read at 450 nm using a SpectraMax i3 Multi-Mode Detection Platform (Molecular Devices LLC, Sunnyvale, CA, USA) and expressed as a percentage of the control.

Immunocytochemical (ICC) analysis

Briefly, BV2 microglia cells fixed on coverslips were rinsed with PBS and pretreated with 0.1% bovine serum albumin (BSA) for 30 min and incubated overnight at 4 °C with a rabbit anti-IL-1ß and IL-18 (1:1000 dilution). Thereafter, the sections were incubated with goat anti-rabbit IgG Alexa 594 or 488 (diluted 1:500) at room temperature for 1 h. Finally, IL-1ß and IL-18 fluorescence intensity/expression in the SNpc was quantified using ImageJ software (Bethesda, MD, USA).

Small interfering RNA (siRNA) transfection and treatment

BV2 microglia cells at 70–80% confluency were seeded in 60 mm dishes and transfected with siRNAs using Lipofectamine 2000. Specifically, the cells were transfected with stealth siRNA using Lipofectamine 2000 (5 μL) mixed with 30 μM of siRNA solution (NLRP3 or scrambled siRNA) and 3 mL of Opti-MEM (Gibco). After incubation at 25 °C for 30 min, a serum-free medium (500 μL) was added to each dish, followed by incubation for 24 h. Thereafter, BV2 microglia cells transfected with siRNA were treated with rebamipide (10 μM) for 12 h, followed by stimulation with α-synuclein and MPP^+ for 11 h. The experimental design timeline is shown in Fig. 4D.

Molecular docking analysis

Molecular docking was performed using AutoDock Vina and Schrödinger Glide to evaluate the binding interactions of rebamipide with key NLRP3 inflammasome-associated proteins. Briefly, the crystal structures of the NLRP3 PYD domain (PDB: 3QF2); ASC PYD domain (PDB: 5H8O); Rb-B7, an ASC-binding nanobody in complex with the CARD domain of ASC (PDB: 5H8O, Chain B); and NLRP3 bound to NEK7 (PDB: 6 NPY, 8SXN) were retrieved from the Protein Data Bank (PDB). Full-length human NLRP3 and human ASC structures were obtained from the AlphaFold Protein Structure Database.

Ligand and protein structures were prepared using the LigPrep and Protein Preparation Wizard modules in Schrödinger for docking analysis, and AutoDockTools was used for grid box generation and ligand optimization. Compounds were docked against NLRP3 using AutoDock Vina and Schrödinger Glide in standard precision (SP) mode, followed by extra precision (XP) rescoring. Binding

affinities were ranked using virtual screening scores, and interactions with key residues were analyzed. The highest-ranked binding pockets were further characterized using the SiteMap module in Schrödinger to predict druggable regions. Molecular docking analysis results were further validated by Surface plasmon resonance analysis to confirm the predicted binding interactions.

Surface plasmon resonance (SPR) analysis

SPR experiments were performed to assess the binding kinetics and affinity of rebamipide for NLRP3 and the NLRP3-NEK7 complex using an iMSPR-mini system (iCLUBIO, Seongnam, Korea) at the Chiral Material Core Facility Center, Sungkyunkwan University. A Nickel-NTA gold (NTA-Au) sensor chip functionalized with His-tag-specific antibodies was utilized to immobilize His-tagged NLRP3 and NLRP3-NEK7 proteins. Before immobilization, the sensor chip was conditioned with 4-(2-hydroxyethyl)−1-piperazineethanesulfonic acid (HEPES)-buffered saline containing 0.05% Tween-20 (HBS-T, pH 7.4), supplemented with 3 mM $CaCl_2$ and 0.6 mM $MgCl_2$. Proteins were immobilized at a flow rate of 20 µL/min for 5 min until a stable baseline was achieved. Rebamipide was dissolved in HBS-T buffer and injected at increasing concentrations (12.5, 25, 50, 100, and 200 µM) to assess its interaction with NLRP3 and the NLRP3-NEK7 complex. Binding interactions were monitored in real-time under continuous flow conditions (20 µL/min), with association and dissociation phases recorded for 400 s each. The sensor chip was regenerated using 0.5 M EDTA and 0.1 M NaOH between experimental cycles, allowing for multiple reuses. Kinetic parameters, including the association rate constant (k_a), dissociation rate constant (k_e), and equilibrium dissociation constant (K^D), were determined using a 1:1 Langmuir binding model in iMSPR analysis software (iCLUBIO). Reference channel data (buffer-only control) was subtracted from all measurements to account for nonspecific binding.

Pharmaco-net analysis

Pharmaco-net analysis was performed to investigate the interactions between the drug, rebamipide, and its target proteins and identify its mechanism of action within biological networks. Drug-related data, including chemical structures (SMILES or InChI) and known target proteins, were obtained from public databases such as DrugBank, PubChem, and UniProt. Protein–protein interaction (PPI) data were retrieved from STRING or BioGRID to construct a comprehensive drug-target network, visualized using Cytoscape. In the network diagram, nodes represent proteins or the drug itself, and edges denote interactions, such as binding or biological associations. Centrality measures, including degree and betweenness centrality, were applied to identify key target proteins and their relative importance within the network. Pathway enrichment analysis was conducted using Kyoto Encyclopedia of Genes and Genomes (KEGG) or Reactome databases to identify the biological pathways most affected by the drug. Additionally, clustering methods were employed to identify functionally related protein modules, enabling the evaluation of multi-target effects. This systems-level approach provided insights into the drug's mechanism of action, highlighting its key target proteins, associated pathways, and potential off-target effects.

Animals

C57BL/6 mice

Male C57BL/6 mice (8-week-old, weighing 23–24 g) were purchased from Doo Yeol Biotech (Seoul, Korea) and maintained under temperature- and light-controlled conditions (20–23 °C, 12 h/12 h light/dark cycle), with food and water provided ad libitum. All animals were acclimatized for 3 or 7 d before drug administration. All animal experiments were approved by the institutional animal care committee of Korea Institute of Oriental Medicine (KIOM) and performed according to the guidelines of the Animal Care and Use Committee at KIOM.

CRISPR/Cas9: generation of NLRP3 knockout (KO) mice

sgRNA synthesis and validation

A single-guide RNA (sgRNA) targeting exon 5 of the NLRP3 gene and Cas9 protein tagged with a nuclear localization signal were procured from Macrogen, Inc. to generate $NLRP3^{KO}$ mice (Fig. 5A). The activity of the sgRNA was validated using in vitro cleavage reactions. Amplified NLRP3 DNA was incubated with 20 nM of Cas9 protein and 40 nM of sgRNA in 1× NEB 3.1 buffer at 37 °C for 90 min. Reactions were terminated using a 6 ×stop solution containing 30% glycerol, 1.2% sodium dodecyl sulfate (SDS), and 100 mM EDTA. The cleavage activity was confirmed via electrophoresis of the reaction mixtures.

Microinjection and knockout (KO) mouse generation

Fertilized embryos were collected from C57BL/6 N female mice, which had been treated with pregnant mare serum gonadotropin (PMSG) and human chorionic gonadotropin (HCG) and mated with C57BL/6 N stud males. Females displaying vaginal plugs were sacrificed to harvest embryos. Thereafter, the sgRNA and Cas9 protein mixture was microinjected into one-cell stage embryos, which were subsequently incubated at 37 °C for 1–2 h before being transplanted into the oviducts of pseudo-pregnant Institute of Cancer Research (ICR) recipient mice. The $NLRP3^{KO}$ mice were backcrossed and bred to be homogeneous before use. All experimental procedures

were conducted under pathogen-free conditions at Macrogen, Inc., with approval from the Institutional Animal Care and Use Committees.

Genotyping and polymerase chain reaction (PCR) analysis

Genomic DNA (gDNA) was extracted from mouse tail tissue to confirm NLRP3^{KO}. Tissue samples (20–30 mg) were incubated in Buffer TL at 55 °C until homogenized, adding Proteinase K to facilitate lysis. Thereafter, the lysate was processed through a silica column, washed sequentially with Buffer BW and Buffer TW, and eluted with Buffer EB. Purified gDNA was used as a template for PCR amplification, targeting exon 5 of the NLRP3 gene. PCR was performed with primers specific for exon 5 using a reaction mixture containing DNase/RNase-free water, 5× High-Q Taq buffer, 5× High-Q GC Enhancer, dNTPs, forward and reverse primers, and High-Q Taq DNA Polymerase. The thermal cycling conditions were as follows: initial denaturation at 98 °C for 30 s, followed by 35 cycles of 98 °C for 10 s, 60 °C for 10 s, and 72 °C for 1 min, with a final extension at 72 °C for 10 min. PCR products were resolved on 2% agarose gels stained with SYBR Green, with expected fragment sizes of 873 bp for the wild type and ~400 bp for the KO allele (Fig. 5D and Supplemental Fig. 1).

Drug administration

C57BL/6

Male C57BL/6 mice were classified into twenty experimental groups ($n = 7$ or 10 per group) to assess the time-dependent effects of rebamipide and/or MCC950 in an MPTP-induced PD model. Experiments were conducted at two separate time points (3 and 7 d after MPTP injection) to evaluate early and later responses. Mice were assigned to 10 groups at each time point, constituting various treatment and time-matched control conditions.

The group allocations were as follows:

- Day 3 post-MPTP groups: (D3-1) control; (D3-2) MPTP; (D3-3) MPTP + rebamipide 5 mg/kg/day; (D3-4) MPTP + rebamipide 10 mg/kg/day; (D3-5) MPTP + rebamipide 20 mg/kg/day; (D3-6) control; (D3-7) MPTP; (D3-8) MPTP + rebamipide 20 mg/kg/day; (D3-9) MPTP + MCC950 10 mg/kg/day; (D3-10) MPTP + rebamipide 20 mg/kg/day + MCC950 10 mg/kg/day.
- Day 7 post-MPTP groups: (D7-1) control; (D7-2) MPTP; (D7-3) MPTP + rebamipide 5 mg/kg/day; (D7-4) MPTP + rebamipide 10 mg/kg/day; (D7-5) MPTP + rebamipide 20 mg/kg/day; (D7-6) control; (D7-7) MPTP; (D7-8) MPTP + rebamipide 20 mg/kg/day; (D7-9) MPTP + MCC950 10 mg/kg/day; (D7-10) MPTP + rebamipide 20 mg/kg/day + MCC950 10 mg/kg/day.

Time-matched control groups were included at each time point to account for potential time-dependent variability in behavioral and molecular analyses. Rebamipide was dissolved in normal saline and orally administered for six consecutive days, whereas mice in the control groups received equivalent volumes of normal saline (0.25 mL) over the same period. MPTP (20 mg/kg; Sigma-Aldrich, St. Louis, MO, USA) was dissolved in saline and intraperitoneally (*i.p.*) administered four times at 2 h intervals on the third day of rebamipide treatment, as previously described. Mice in groups 1–5 and 11–15 were sacrificed 3 d post-MPTP administration, whereas those in groups 6–10 and 16–20 were sacrificed 7 d post-MPTP administration. The experimental design timeline is shown in Figs. 2A and 4F.

CRISPR/Cas9: generation of NLRP3 KO mice

Male C57BL/6 mice were classified into sixteen experimental groups ($n = 5$ per group) to evaluate the effects of rebamipide in NLRP3^{KO} models of PD following MPTP administration. All experiments were conducted at a single time point 3 d after MPTP injection to investigate early pathological and behavioral responses. Mice were assigned to eight Cas9^{Ctrl} groups and eight NLRP3^{KO}groups, each including vehicle control and two doses of rebamipide treatment.

The group allocations were as follows:

- Day 3 post-MPTP groups: (CR-D3-1) Ctrl-control; (CR-D3-2) Ctrl-MPTP; (CR-D3-3) Ctrl-MPTP + rebamipide 10 mg/kg/day; (CR-D3-4) Ctrl-MPTP + rebamipide 20 mg/kg/day; (CR-D3-5) KO-control; (CR-D3-6) KO-MPTP; (CR-D3-7) KO-MPTP + rebamipide 10 mg/kg/day; (CR-D3-8) KO -MPTP + rebamipide 20 mg/kg/day;
- Day 7 post-MPTP groups: (CR-D7-1) Ctrl-control; (CR-D7-2) Ctrl-MPTP; (CR-D7-3) Ctrl-MPTP + rebamipide 10 mg/kg/day; (CR-D7-4) Ctrl-MPTP + rebamipide 20 mg/kg/day; (CR-D7-5) KO-control;(CR-D7-6) KO-MPTP; (CR-D7-7) KO-MPTP + rebamipide 10 mg/kg/day; (CR-D7-8) KO-MPTP + rebamipide 20 mg/kg/day. Time-matched control groups were included at each time point to account for potential time-dependent variability in behavioral and molecular analyses.

Rebamipide was dissolved in normal saline and orally administered for six consecutive days, with the control groups receiving equivalent volumes of normal saline (0.25 mL) over the same period. MPTP (20 mg/kg;

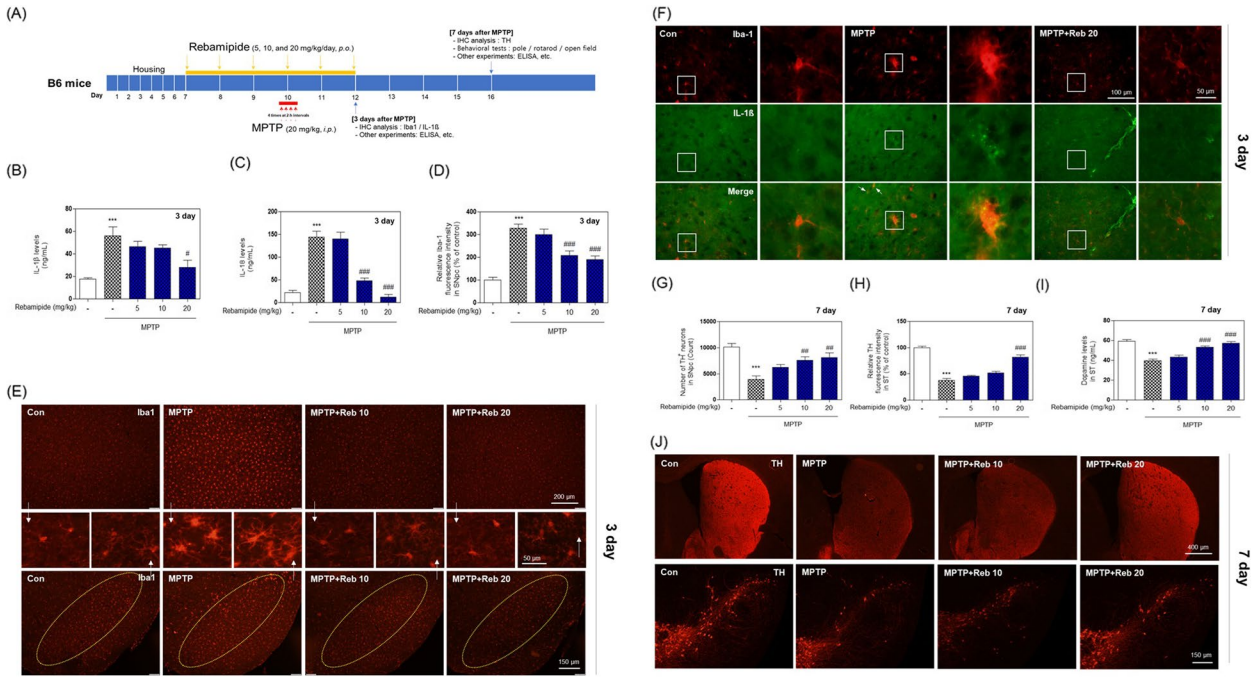

Fig. 2 Overview of the experimental design. **A** Inhibitory effects of rebamipide on 1-methyl-4-phenyl-1,2,3,6-tetrahydropyridine (MPTP)-induced upregulation of IL-1ß (**B** and **F**) and IL-18 (**C**), and microglia activation (**D**, **E**, and **F**) in the mouse substantia nigra pars compacta (SNpc) 3 d after MPTP injection. Dopaminergic neurons were visualized 7 d after the last MPTP treatment using tyrosine hydroxylase (TH)-specific immunostaining. TH-immunopositive neurons in the SNpc were counted (**G**), and the relative TH fluorescence intensity in the striatum (ST) was measured (**H**). Dopamine levels in the ST were measured using HPLC (**I**). Representative photomicrographs of the SNpc and ST (**J**). Data are presented as the mean ± standard error of mean (SEM). * $p < 0.05$, ** $p < 0.01$, ***$p < 0.001$, compared with the control group; # $p < 0.05$, ## $p < 0.01$, ### $p < 0.001$, compared with the MPTP-treated group

Sigma-Aldrich, St. Louis, MO, USA) was intraperitoneally (*i.p.*) administered four times at 2 h intervals on the third day of rebamipide treatment, as previously described. Mice in groups 1–8 were sacrificed 3 d post-MPTP administration, whereas those in groups 9–16 were sacrificed 7 d post-MPTP administration. The experimental design timeline is shown in Fig. 5E.

Behavioral tests

Behavioral tests were conducted according to previously published methods. Briefly, the pole test was performed on the seventh day following the last MPTP injection. Specifically, the mice were held on the top of the pole (diameter 8 mm, height 55 cm, with a 6 rough surface), and the time needed for the mice to descend with all four feet on the floor was recorded, with a 30 s cutoff limit. Each trial had a cutoff limit of 50 s.

Moreover, the rotarod test was performed on the seventh day following the last MPTP injection. The rotarod unit constitutes a rotating spindle (7.3 cm diameter) and five individual compartments. After two or three training sessions, the rotation speed was increased to 10–30 rpm (acceleration mode) in a test session. The time each mouse remained on the rotating bar was recorded over three trials, with a maximum duration of 5 min per trial. Data were presented as the mean time on the rotating bar across the three test trials.

The open field test was performed between 9 P.M. and 2 A.M. to avoid diurnal variation. Briefly, the mice were placed in the testing chamber (40 ×25 ×18 cm) with white floors and recorded for 30 min using a computerized automatic analysis system (Viewer; Biobserve, Bonn, Germany). Data collected by the computer included the total distance traveled, determined by tracking the center of the animal.

Brain tissue preparation, immunohistochemical (IHC) and ELISA

The mice in the groups were anesthetized at 3 and 7 d following either saline or MPTP treatment and subjected to transcardial perfusion with 0.05 M PBS and cold 4% paraformaldehyde (PFA) in 0.1 M phosphate buffer (PB). Thereafter, mouse brains were extracted and post-fixed in a 0.1 M PB solution containing 4% PFA overnight at 4 °C. To ensure cryoprotection, the brain samples were immersed in a solution containing 30% sucrose in 0.05 M PBS, cut into serial 30 µm-thick coronal sections using a freezing microtome, and stored

in cryoprotectant solution at 4 °C until IHC analysis. IHC assays were performed according to previously described procedures [25]. Dopaminergic neurons in the SNpc were assessed by analyzing coronal sections approximately 3.28 mm posterior to the bregma (−2.54 ~ −4.04 mm) [25]. Further, brain sections were sampled at approximately 0.62 mm anterior to the bregma (0.98 ~ 0.50 mm) to analyze the intensity of striatal TH-positive nerve fibers [25]. Briefly, the sections were incubated overnight at 4 °C with antibodies targeting TH (TH; diluted 1:2000) or Iba-1 (Iba-1; diluted 1:500), 0.3% Triton X-100, 0.5 mg/mL BSA, and 2% NGS. Thereafter, the sections were incubated with goat anti-rabbit IgG Cy3 conjugate Alexa 594 (diluted 1:500) (diluted 1:100) at room temperature for 1 h. The tissue sections were subsequently placed on gelatin-coated slides, dehydrated using an ascending alcohol series, cleared using xylene, and covered with fluorescence mounting medium. Quantitative analysis of TH-immunoreactive (IR) cells in the SNpc and optical intensity of TH-IR in the striatum (ST) was performed at × 100 and × 40 magnifications, respectively, using Stereo-investigator software (MBF Bioscience Inc., Williston, VT, USA). Additionally, microglial activation in the SNpc or ST was assessed at × 100 magnification using Stereo-investigator software (MBF Bioscience Inc., Williston, VT, USA). Notably, the results were presented as percentages relative to control group values. Images were captured using a research microscope (BX53; Olympus Corporation, Tokyo, Japan). Image-based quantification of mouse tissue regions was conducted using ImageJ 1.50i software (National Institutes of Health, Bethesda, MD, United States).

Next, brain sections were rinsed with PBS and incubated with a mouse anti-IL-1ß antibody (diluted 1:100) to assess the co-localization patterns of Iba-1/IL-1ß. Thereafter, the tissues were treated with a goat anti-mouse IgG conjugate Alexa 488 (diluted 1:500) and incubated with a rabbit anti-Iba-1 antibody (diluted 1:500). The sections were rinsed with PBS and incubated with biotinylated anti-rabbit IgG (diluted 1:200), followed by treatment with streptavidin-Alexa 594 (diluted 1:200) for 1 h. The tissue sections were mounted on gelatin-coated slides and covered with fluorescence mounting medium. Images were captured at 400 × magnification using a fluorescence microscope (for Iba-1/IL-1ß co-localized images) (Olympus Microscope System BX53; Olympus, Tokyo, Japan), equipped with a 40 × objective lens. Results were presented as percentages of control group values. Image quantification of mouse tissue regions was performed using ImageJ 1.50i software (National Institutes of Health, Bethesda, MD, United States).

The BV2 microglia cells, supernatants, and SNpc were rapidly dissected, homogenized, and centrifuged using standard laboratory techniques for ELISA. The resulting supernatants were stored at -80 °C until further use. ELISA kits were used for quantification, according to the manufacturer's instructions.

Stereological and fluorescence-based quantification of th expression

Quantification of dopaminergic neurons in the SNpc was performed using an unbiased stereological approach. Imaging and analysis were conducted using the BioQuant Nova Prime system (BioQuant Imaging, Nashville, TN), integrated with an Olympus BX-50 microscope (Olympus Optical, Tokyo, Japan), motorized stage, and a Retiga-cooled charge-coupled device (CCD) camera (Q-Imaging, Burnaby, BC, Canada). Coronal brain sections were collected from regions anterior to the SNpc (starting at bregma, −2.54 mm) to the level of the pontine nuclei (approximately bregma, −4.04 mm), according to the stereotaxic mouse brain atlas [26]. Each section of the ventral midbrain was initially examined at low magnification (10 × objective) to outline the SNpc, which was distinguished from the ventral tegmental area using anatomical landmarks, such as the third cranial nerve and cerebral peduncle. Neurons were subsequently counted under high magnification (80 × objective), including only TH-positive neurons with clearly identifiable nuclei, nucleoli, and cytoplasmic boundaries. TH expression in the ST was quantified based on the area of TH-positive staining. Relative intensity was measured using ImageJ software by calculating the integrated fluorescence (IF) intensity after background subtraction. The results were normalized and expressed as a percentage of control group values. Final neuron counts were estimated based on the optical fractionator method described by Gundersen and Jensen (1987) [25].

Dopamine level measurements using high-performance liquid chromatography (HPLC)

Briefly, dopamine levels of the brain tissues were estimated using UPLC-MS/MS (SCIEX ExionLC series UHPLC and SCIEX Triple Quadrupole 6500 +), coupled with an electrochemical detection system. The ST was identified (bregma 1.42 ~ 0.10 mm) according to the mouse brain atlas and was dissected using previously reported methods. Thereafter, the ST tissue was homogenized in 1% formic acid and centrifuged at 14,000 g for 10 min to collect the supernatant, which was filtered

through a 0.22-μm membrane. An aliquot (10 μL) of the resulting solution was injected into the HPLC pump. Chromatographic separation was performed using an Acquity UPLC HSS T3 column (2.1 ×100 mm, 1.8 μm; Waters, Milford, MA, USA). The composition of the mobile phase was as follows: solvent A, water, 0.1% formic acid, and 5 mM ammonium formate; and solvent B, CAN/MeOH (v/v, 1:1, 5 mM ammonium formate). The flow rate was maintained at 0.3 mL/min, and the column temperature was maintained at 30 °C. Dopamine standards were prepared in 1% formic acid, and each concentration was adjusted relative to the standard and quantified from a standard curve. Dopamine levels were calculated as nanograms per microgram of total protein. Protein quantification was performed using the Bradford protein assay kit (Bio-Rad, Hercules, CA, USA), according to the manufacturer's instructions.

Statistical analysis

All statistical analyses were conducted using GraphPad Prism 7.0 software (GraphPad Software, San Diego, CA, USA). Data were expressed as mean ± standard error of the mean (SEM). Significant differences between the treatment groups were determined using one-way analysis of variance, followed by Tukey's post-hoc tests for multiple comparisons. Statistical significance was set at $p < 0.05$.

Results

Rebamipide inhibits α-synuclein and MPP+-induced NLRP3 inflammasome-related neuroinflammatory cytokines in BV2 microglial cells

Lactate dehydrogenase (LDH) assay was performed to investigate the protective effect of rebamipide against α-synuclein and MPP^+-induced cytotoxicity in microglia BV2 cells (Fig. 1). While rebamipide was cytotoxic to BV2 microglia cells at a concentration of 50 μM, it was safe at concentrations ranging from 0.001–10 μM after 12 h of treatment (Fig. 1C). Incubation with α-synuclein and MPP^+ increased LDH levels in BV2 microglia cells compared to those in the control group. Moreover, in vivo studies showed no dopaminergic neuronal death at doses up to 20 mg/kg, suggesting the safety of rebamipide within this range (Supplemental Fig. 2). Based on these results, all further experiments were performed using 0.001–10 μM of rebamipide. Additionally, we investigated the effect of rebamipide on the levels of neuroinflammatory cytokines in BV2 microglia cells. Rebamipide suppressed IL-1β and IL-18 secretion (Fig. 1F-I) and cell toxicity induced by α-synuclein and MPP^+ but did not significantly influence tumor necrosis factor (TNF)-α and IL-6 levels (Fig. 1D and E). Subsequently, we examined the effect of rebamipide on NLRP3 inflammasome levels in BV2 microglia cells. We used ELISA to assess its inhibitory effects on NLRP3 inflammasome (J) and p20 (M) in microglial BV2 cells. As shown in Fig. 1J-M, α-synuclein and MPP^+ induced the expression of NLRP3, ASC, procaspase-1, and p20. Rebamipide treatment reduced NLRP3 inflammasome and p20 secretion and slightly decreased pro-caspase-1 levels. However, it did not significantly affect ASC levels.

Rebamipide directly binds the NLRP3-NEK7 complex and modulates NLRP3 inflammasome activity

Molecular docking was conducted using AutoDock Vina and Schrödinger Maestro to assess the potential inhibitory effects of rebamipide on NLRP3 inflammasome activation. Structure-based virtual screening was performed to evaluate the binding affinity of rebamipide for key NLRP3 inflammasome components, including the NLRP3-NEK7 complex, full-length NLRP3, full-length ASC, NLRP3 PYD domain, and ASC CARD domain (Supplemental Fig. 3). Molecular docking analysis showed that rebamipide exhibited the strongest binding affinity for the NLRP3-NEK7 complex, followed by full-length NLRP3 and full-length ASC (Table 1). Notably, rebamipide engaged in simultaneous hydrogen bonding and halogen interactions with NLRP3 and NEK7, suggesting a potential role in disrupting or stabilizing their interaction (Fig. 1N). SPR analysis was performed to determine the binding kinetics of rebamipide with NLRP3 and the NLRP3-NEK7 complex to validate these in silico findings. Importantly, the binding affinity of rebamipide with NLRP3 and the NLRP3-NEK7 complex

Table 1 Molecular docking affinity of rebamipide with NLRP3 inflammasome-associated proteins

Compound	Target protein	Affinity (kcal/mol)
Rebamipide	NLRP3 and NEK7 complex [PDB: 6NPY]	−10.5
	NLRP3 and NEK7 complex [PDB: 8SXN]	−8.4
	Full-length NLRP3 [Alphafold Model: AF-Q96P20-F1-v4]	−5.5
	Full-length ASC [Alphafold Model: AF-Q9ULZ3-F1-v4]	−4.8
	NALP3 PYD domain [PDB: 3QF2]	−4.8
	ASC CARD domain [PDB: 5H8O] (chain A deletion)	−4.2

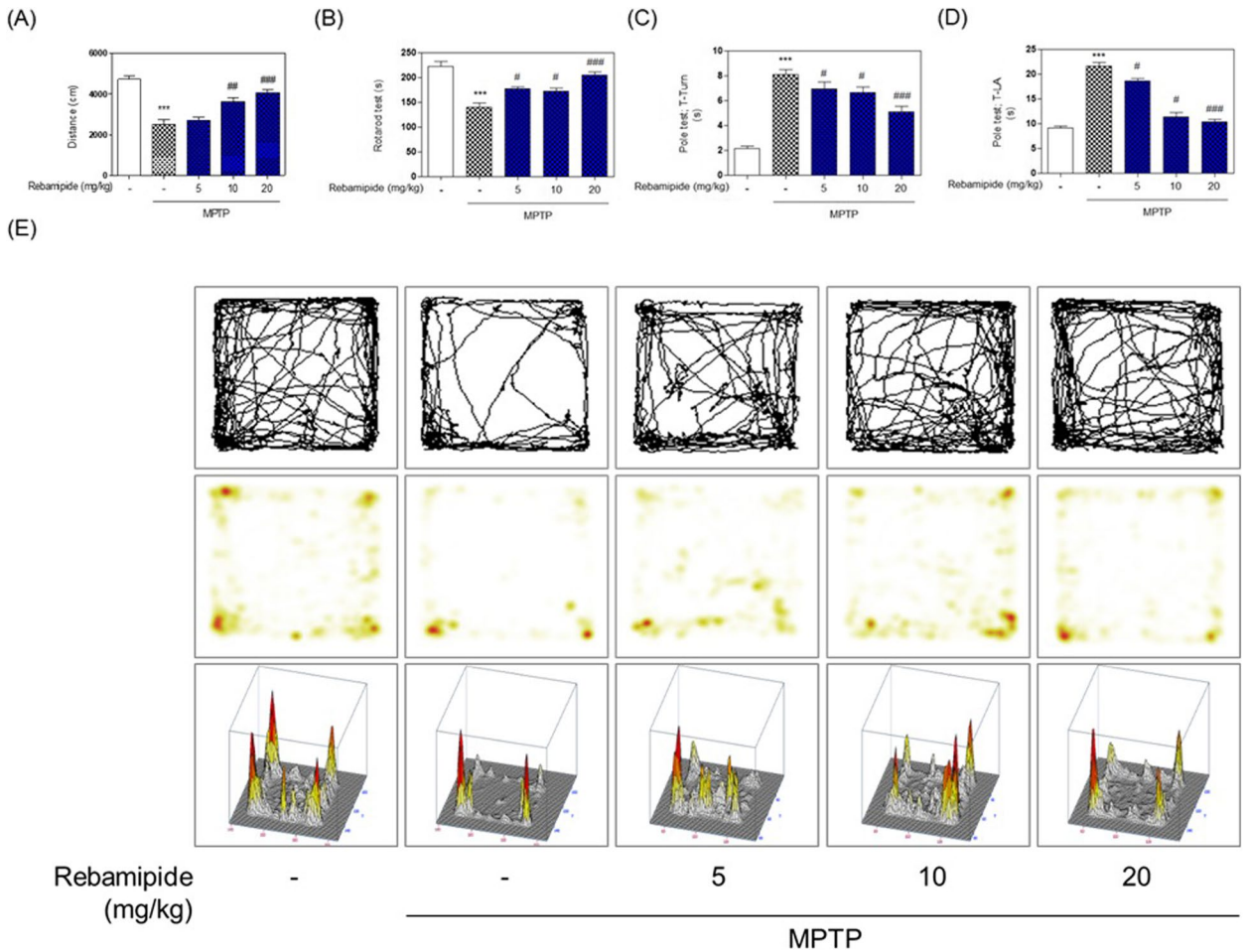

Fig. 3 Protective effects of rebamipide on 1-methyl-4-phenyl-1,2,3,6-tetrahydropyridine (MPTP)-induced motor deficits in mice. Rebamipide was administered for 5 d. Representative images of mouse movement in the open field box, as captured by the video tracking system. The total distance covered by the mice was quantified in the open field box 7 d after MPTP injection (**A** and **E**). Latency time on the rotarod was recorded 7 d after MPTP injection, with a 300 s cutoff limit (**B**). The time it took to turn completely downward (**C**) and the time to fall off the rod onto the floor (**D**) were recorded 7 d after MPTP injection, with a 60 s cutoff limit. Data are presented as mean ± standard error of mean (SEM). * $p < 0.05$, ** $p < 0.01$, ***$p < 0.001$, compared with the control group; # $p < 0.05$, ## $p < 0.01$, ###$p < 0.001$, compared with the MPTP-treated group

increased with increasing concentrations of rebamipide (Fig. 1O and P). Collectively, these results indicated that rebamipide directly interacts with the NLRP3-NEK7 complex, supporting its potential role as an NLRP3 inflammasome modulator.

Rebamipide suppresses NLRP3-induced neuroinflammatory cytokines in BV2 microglial cells

Treatment with the NLRP3 inflammasome activators ATP, nigericin, and the toxin gramicidin induced caspase-1 activation and IL-1β secretion (Fig. 1R-T). In contrast, rebamipide inhibited IL-1β secretion induced by the NLRP3 inflammasome activators in a dose-dependent manner (Fig. 1U–X).

Rebamipide reduces NLRP3 inflammasome-related microglial activation in the MPTP mouse model

We quantified Iba-1, IL-1β, and IL-18 levels in ST and SNpc in mouse brains to confirm the inhibitory effects of rebamipide on microglial activation and NLRP3 inflammasome-related cytokines (Fig. 2). IL-1β and IL-18 levels were upregulated in MPTP-treated mice compared to those in the control group. However, rebamipide treatment (10–20 mg/kg) significantly downregulated these cytokines (Fig. 2B and C). Additionally, rebamipide treatment (10–20 mg/kg) significantly suppressed MPTP-induced upregulation of microglial activation (Fig. 2D and E). Immunofluorescence assay showed that rebamipide treatment (20 mg/kg/day) significantly suppressed the number of Iba-1/IL-1β

double-positive cells in the SNpc following MPTP stimulation (Fig. 2F).

Rebamipide protects against dopaminergic neuronal loss and dopamine depletion in the MPTP mouse model

IHC assays were performed to examine TH levels in the SNpc and ST of mouse brains to investigate the effects of rebamipide on dopaminergic neuronal death. While a significant decrease was observed in TH-positive cells and fibers in the SNpc and ST of MPTP-treated mice, rebamipide treatment (10–20 mg/kg) significantly increased the cells (Fig. 2G, H, and J). Additionally, we examined dopamine levels in the ST of mouse brains to elucidate the effect of rebamipide on dopamine levels. Rebamipide treatment significantly reversed the MPTP-induced decrease in dopamine levels (Fig. 2I).

Rebamipide alleviates MPTP-induced motor deficits

An open-field test was performed to examine the effect of rebamipide on MPTP-induced changes in motor function (Fig. 3). While MPTP significantly decreased the distance traveled by mice on day 7, rebamipide treatment significantly increased the distance traveled (Fig. 3A and E). Additionally, a rotarod test was performed to examine the effect of rebamipide on MPTP-induced motor incoordination and postural imbalance. MPTP significantly decreased the retention time compared to that in the control group. However, rebamipide treatment significantly increased the retention time in the rotarod test (Fig. 3B). Additionally, we performed a pole test to investigate the effect of rebamipide on MPTP-induced bradykinesia and found that rebamipide significantly shortened T-turn and T-LA times (Fig. 3C and D).

NLRP3 inhibition neutralizes the inhibitory effect of rebamipide on NLRP3 inflammasome signaling in α-synuclein and MPP+-intoxicated BV2 microglia cells

Rebamipide treatment significantly suppressed microglial activation, NLRP3 inflammasome signaling, and IL-1β and

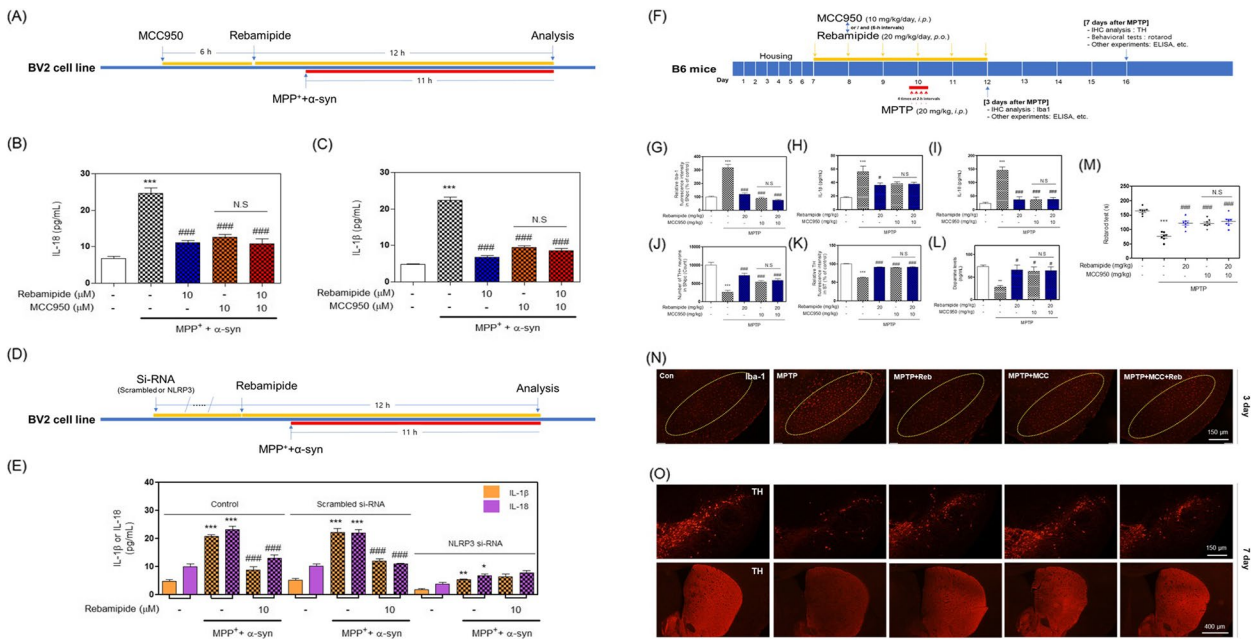

Fig. 4 NLRP3 inhibition neutralizes the protective effect of rebamipide following α-synuclein + MPP^+ intoxication. Overview of the experimental design. **A** BV2 microglia cells were treated with NLRP3 inflammasome inhibitor (MCC950) for 6 h, treated with rebamipide for 1 h, and stimulated with α-synuclein + MPP^+ for an additional 11 h. IL-1ß (**B**) and IL-18 (**C**) levels were evaluated using enzyme-linked immunosorbent assay kits (ELISA). Overview of the experimental design (**D**). Effects of NLRP3 on IL-1ß and IL-18 regulation (**E**) in NLRP3 siRNA-transfected BV2 microglia cells. NLRP3 inhibition neutralized the protective effect of rebamipide following 1-methyl-4-phenyl-1,2,3,6-tetrahydropyridine (MPTP) intoxication. An MCC950 or saline was injected once daily in the MPTP intoxication model before rebamipide treatment. Overview of the experimental design. **F** Microglial activations were visualized 3 d after the last MPTP treatment using Iba-1-specific immunostaining. Iba-1-immunopositive microglia in the substantia nigra pars compacta (SNpc) were counted 3 d after the last MPTP treatment (G and N). IL-1ß (H) and IL-18 (**I**) levels were evaluated using enzyme-linked immunosorbent assays (ELISA). Moreover, dopaminergic neurons were visualized 7 d after MPTP injection, using tyrosine hydroxylase (TH)-specific immunostaining. TH-immunopositive neurons in the SNpc (**J** and **O**) were counted, and the relative TH fluorescence intensity in the striatum (ST) (**K** and **O**) was measured. Dopamine levels in the ST were measured using HPLC (**L**). Latency time on the rotarod was recorded 7 d post-MPTP injection, with a 300 s cutoff limit (**M**). Data are expressed as mean ± standard error of the mean (SEM). * $p < 0.05$, ** $p < 0.01$, *** $p < 0.001$, compared with the control group; # $p < 0.05$, ## $p < 0.01$, ### $p < 0.001$, compared with the α-synuclein + MPP + or MPTP-treated group

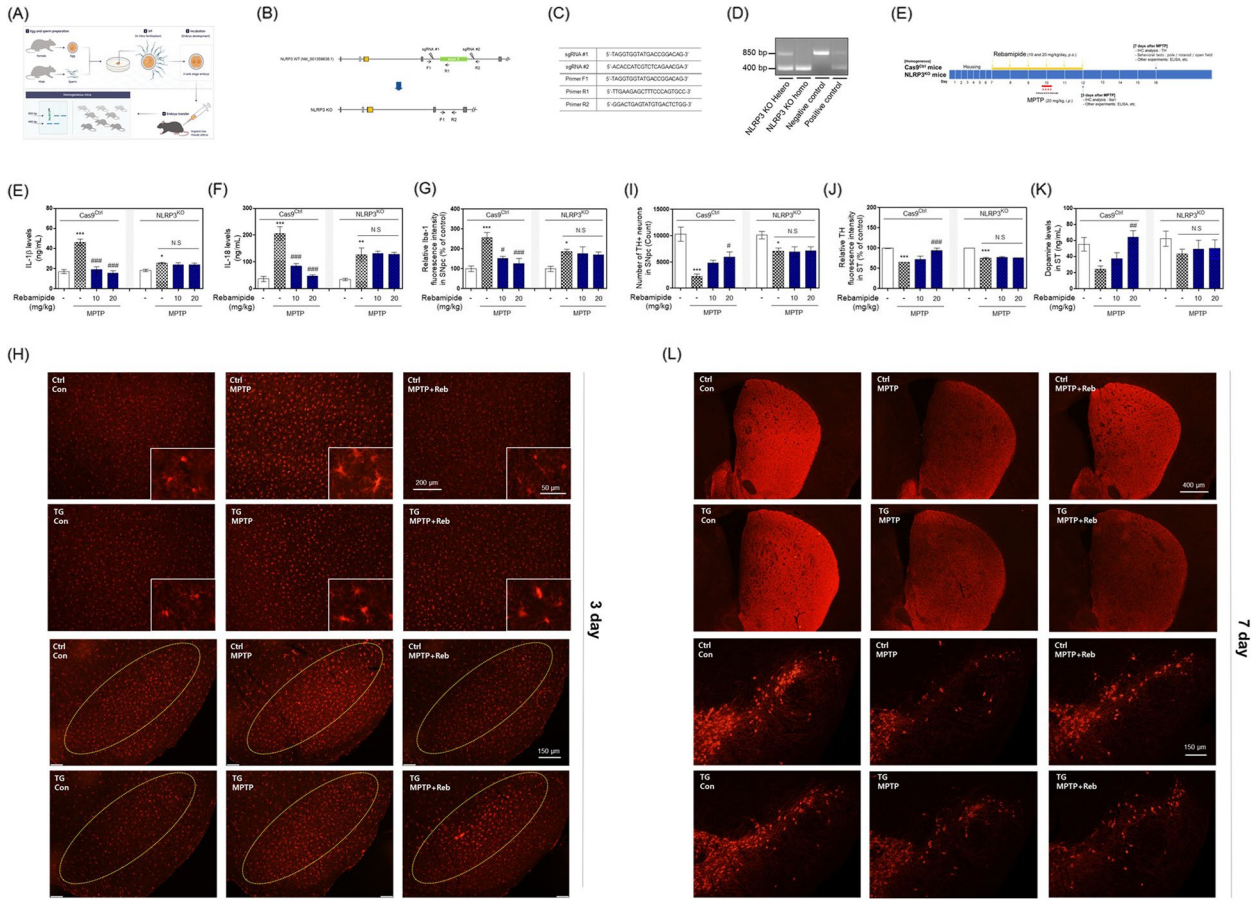

Fig. 5 NLRP3^{KO} using CRISPR/Cas9 neutralizes the protective effect of rebamipide following 1-methyl-4-phenyl-1,2,3,6-tetrahydropyridine (MPTP) intoxication. Schematic of the NLRP3^{KO} using CRISPR/Cas9 (**A**) Sequences for CRISPR-Cas9 (**B**) and primer sequences for real-time RT-PCR (**C**) NLRP3^{KO} (hetero or homo) was confirmed using real-time PCR (**D**) Overview of the experimental design (**E**). Inhibitory effects of rebamipide on MPTP-induced levels of IL-1ß (**E**), IL-18 (**F**), and microglia activation (**G** and **H**) in the substantia nigra pars compacta (SNpc) 3 d after MPTP injection. Moreover, dopaminergic neurons were visualized using tyrosine hydroxylase (TH)-specific immunostaining 7 d after the last MPTP treatment. TH-immunopositive neurons in the SNpc were counted (**I**), and the relative TH fluorescence intensity in the striatum (ST) was measured (**J**). Dopamine levels in the ST were measured using HPLC (**K**). Representative photomicrographs of the SNpc and ST (**L**). Data are expressed as mean ± standard error of the mean (SEM). *$p < 0.05$, **$p < 0.01$, ***$p < 0.001$, compared with the control group; # $p < 0.05$, ## $p < 0.01$, ###$p < 0.001$, compared with the MPTP-treated group

IL-18 secretion induced by α-synuclein and MPP$^+$ intoxication. Collectively, these results suggested that NLRP3 inflammasome signaling plays a pivotal role in mediating the protective effects of rebamipide against MPTP-induced neurotoxicity. BV2 microglia cells were treated with the NLRP3 inflammasome inhibitor MCC950 and rebamipide in the presence of α-synuclein and MPP$^+$ to further investigate rebamipide's mechanism of action. Rebamipide demonstrated protective effects against α-synuclein- and MPP$^+$-induced neurotoxicity, as anticipated (Fig. 4A–C). However, these protective effects were abolished following preinhibition of NLRP3 inflammasome signaling and IL-1β and IL-18 secretion by MCC950. Subsequently, siRNA-mediated knockdown of NLRP3 expression was performed to confirm these observations (Fig. 4D and E). NLRP3 suppression neutralized the protective effects of rebamipide, indicating that NLRP3 inflammasome signaling is crucial for the neuroprotective effect of rebamipide in α-synuclein and MPP$^+$-induced models. These findings indicated that inhibition of NLRP3 signaling attenuated the effects of rebamipide, suggesting that its actions depend on the NLRP3 inflammasome.

MCC950-induced NLRP3 inhibition neutralizes the effect of rebamipide on motor deficits via microglial activation and inflammasome signaling in MPTP mouse model

MCC950 (NLRP3 inflammasome inhibitor) neutralized the effects of rebamipide on dopaminergic neurons and

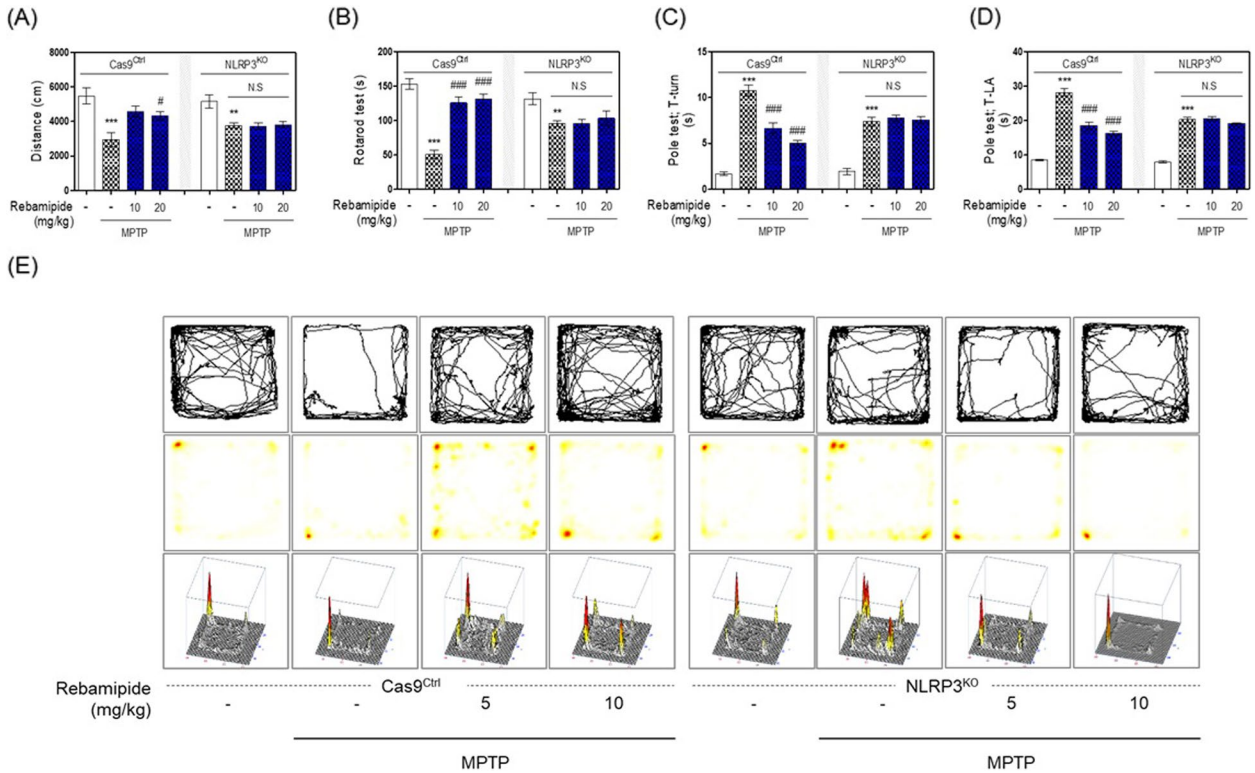

Fig. 6 NLRP3^{KO} neutralizes rebamipide's protective effects on 1-methyl-4-phenyl-1,2,3,6-tetrahydropyridine (MPTP)-induced motor impairment in Cas9^{Ctrl} and NLRP3^{KO} mice. Representative images of mouse movement in the open field box, as captured by the video tracking system. The total distance covered by the mice was quantified in the open field box 7 d after MPTP injection (**A** and **E**), and the latency time on the rotarod was recorded, with a 300 s cutoff limit (**B**). Moreover, the time it took to turn completely downward (**C**) and the time to fall off the rod onto the floor (**D**) were recorded 7 d postinjection, with a 60 s cutoff limit. Data are presented as the mean ± standard error of the mean (SEM). * $p < 0.05$, ** $p < 0.01$, ***$p < 0.001$, compared with the control group; # $p < 0.05$, ## $p < 0.01$, ###$p < 0.001$, compared with the MPTP-treated group

dopamine in the MPTP mouse model. Mice with MPTP-induced PD were injected with MCC950 (*i.p.*) 30 min before treatment with rebamipide or saline to confirm the role of NLRP3 signaling on dopaminergic neurons and PD-related motor deficits (Fig. 4F). Specifically, microglial activation and expressions of NLRP3 inflammasome-related cytokines (IL-1β and IL-18) in the SNpc were examined. Consistent with the in vitro experimental results, MPTP treatment increased microglial activation and NLRP3 inflammasome-related cytokines, which were attenuated by rebamipide (Fig. 4G–I). Additionally, MCC950 pretreatment neutralized the protective effects of rebamipide. However, no significant difference was observed between the rebamipide-treated and MCC950-pretreated groups, indicating that rebamipide exerts its effects via NLRP3 signaling-mediated regulation of inflammasome and microglial activation. Additionally, MCC950 neutralized the rebamipide-mediated protective effect in dopaminergic neurons, with no significant difference between the rebamipide- and MCC950-treated groups (Fig. 4J-L and N). Notably, this pattern was additionally observed in the study of PD-related motor deficits (Figure M).

NLRP3 inhibition reverses the protective effects of rebamipide on dopaminergic neurons and motor deficits in MPTP-intoxicated CRISPR/Cas9 NLRP3 KO mice

We generated NLRP3^{KO} mice using CRISPR/Cas9 gene editing to further investigate the role of NLRP3 inflammasome in the anti-PD effects of rebamipide (Fig. 5A–D). MPTP administration induced notable neurological changes in NLRP3^{Ctrl} mice, which were significantly ameliorated by rebamipide (Fig. 5E). In contrast, MPTP-induced neurotoxicity was less pronounced in NLRP3^{KO} mice, although appropriate induction occurred. Additionally, rebamipide treatment did not show any therapeutic effect in NLRP3^{KO} mice (Fig. 5E–L and Fig. 6A–E). Overall, these results suggested that rebamipide exerts anti-inflammatory effects through the NLRP3 inflammasome in MPTP-induced PD mice, protecting dopaminergic neurons and improving PD-related motor deficits.

Discussion

Microglial activation is increasingly recognized as a primary contributor to dopaminergic neurodegeneration in PD [21]. Activated microglia secrete proinflammatory

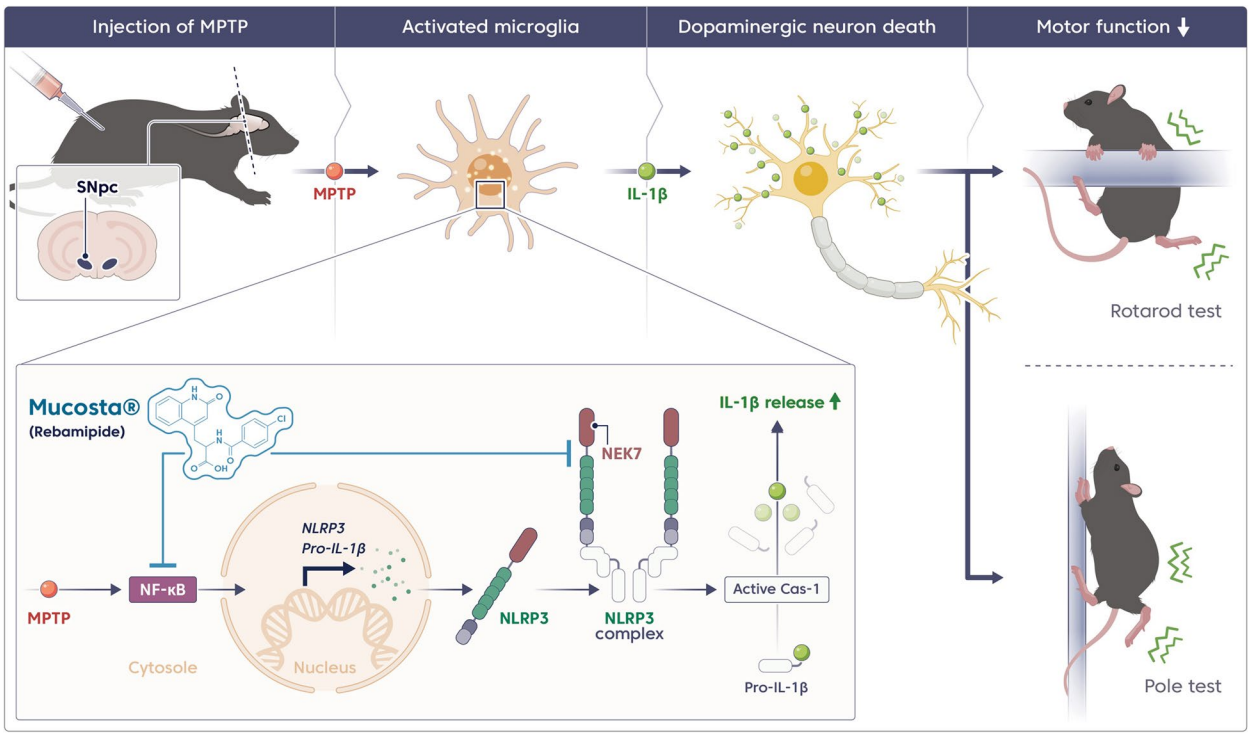

Fig. 7 Proposed mechanism through which rebamipide protects via NLRP3 inhibition against Parkinson's disease pathogenesis. Rebamipide (Mucosta®), a clinically approved drug, alleviates neuroinflammation and dopaminergic neurodegeneration in a Parkinson's disease model

cytokines such as TNF-α, IL-1β, and IL-6, which are elevated in the cerebrospinal fluid and brains of PD patients, particularly within the ST [21, 22]. These cytokines impair dopaminergic signaling and promote neuronal death, especially during the early stages of disease progression [22]. In our study, rebamipide treatment significantly reduced IL-1β levels in both BV2 microglia and MPTP-induced mouse models, suggesting that modulation of microglial activity contributes to its neuroprotective effects. The phenotypic plasticity of microglia shifting between the proinflammatory M1 and anti-inflammatory M2 states plays a dual role in PD pathogenesis [23, 24]. Rebamipide appears to promote a shift away from the M1 phenotype, as evidenced by decreased IL-1β expression, without significantly altering TNF-α or IL-6 levels [23–26]. This selective suppression may be sufficient to relieve dopaminergic toxicity, given IL-1β known potency in disrupting neuronal function [23, 24, 27, 28]. A mechanistic link between neuroinflammation and dopaminergic preservation was further supported by behavioral improvements in MPTP-treated mice [29, 30]. Rebamipide administration led to enhanced performance in the rotarod and pole tests, which correlated with increased survival of TH-positive neurons in the SNpc. This suggests that functional restoration of the nigrostriatal pathway underlies the observed motor improvements. At the molecular level, our findings highlight the inhibition of the NLRP3 inflammasome as a key therapeutic mechanism of rebamipide. NLRP3 functions as an innate immune sensor, triggering caspase-1 activation and IL-1β release upon stimulation [31–33]. Chronic activation of this pathway leads to sustained neuroinflammation and pyroptotic cell death [34, 35]. Rebamipide significantly attenuated the expression of NLRP3 and pro-IL-1β in BV2 cells and SNpc, possibly through suppression of NF-κB signaling (Supplemental Fig. 4), thereby disrupting a central inflammatory cascade [36, 37]. Importantly, we identified that rebamipide directly interferes with the NLRP3-NEK7 interaction, a critical step in inflammasome assembly. Molecular docking indicated binding to the LRR domain of NLRP3, and SPR confirmed dose-dependent interaction. This blockade likely prevents ASC recruitment, caspase-1 activation, and subsequent IL-1β maturation [38]. These findings position rebamipide as a direct inhibitor of inflammasome activation at a structural interface, rather than acting solely through upstream signaling. Consistent with these molecular changes, rebamipide preserved dopaminergic neurons and striatal dopamine levels, supporting a mechanistic link

between inflammasome inhibition and motor function recovery. Notably, rebamipide did not affect IL-1 receptor expression on neurons, indicating that its protective effects occur upstream, at the level of cytokine maturation and release rather than receptor antagonism (Supplemental Fig. 5). Taken together, these results suggest that rebamipide acts through a multimodal mechanism suppressing microglial activation, inhibiting inflammasome assembly, and preserving dopaminergic neurons to exert therapeutic effects in PD. The behavioral improvements observed are thus mechanistically linked to molecular suppression of neuroinflammation, particularly via NLRP3-dependent pathways. Furthermore, loss of rebamipide efficacy under NLRP3 knockdown or inhibition confirms the specificity of its mode of action.

Despite these promising findings, this study had several limitations. First, while rebamipide demonstrated neuroprotective effects, its toxicity at higher concentrations warrants further investigation and dose optimization. Second, the therapeutic potential of rebamipide was not assessed across multiple PD models. Beneficial effects were observed in the 6-OHDA model; nevertheless, the role of NLRP3 inflammasome inhibition in this context remains unexplored. Third, we did not validate the mechanism using NLRP3 knock-in or knockout mice, which would further strengthen the causal link between rebamipide and NLRP3 pathway modulation. Future studies are warranted to evaluate the long-term safety, pharmacokinetics, and therapeutic efficacy of rebamipide in diverse neurodegenerative disease models [39, 40]. Despite these limitations, the established clinical use of rebamipide supports its potential for rapid translational application. Our results highlight that disrupting the NLRP3-NEK7 interaction may be a promising therapeutic strategy for suppressing neuroinflammation in PD.

Conclusions

This study demonstrated that rebamipide exerts NLRP3-dependent anti-inflammatory and neuroprotective effects in BV2 microglia and an MPTP-induced mouse model of PD, suggesting its potential as a treatment for NLRP3-driven neurodegenerative conditions (Fig. 7).

Supplementary Information

The online version contains supplementary material available at https://doi.org/10.1186/s12974-025-03461-z.

Supplementary Material 1: Figure S1. Sequences for CRISPR-Cas9 and genotyping

Supplementary Material 2: Figure S2. Effects of rebamipide on neurotoxicity in the substantia nigra pars compactain mouse brains

Supplementary Material 3: Figure S3. Molecular docking of rebamipide with key domains of the NLRP3 complex. Molecular docking simulations were performed to evaluate the interaction between rebamipide and critical domains of the NLRP3 inflammasome complex. The left panels represent 3D docking models, whereas the right panels display corresponding 2D interaction diagrams.NLRP3 NACHT domain,Apoptosis-associated speck-like protein containing a CARDfull-length structure,NEK7 kinase domain,NLRP3 PYD domain. Hydrogen bonding interactions are indicated by purple arrows, whereas salt bridges are represented by red and blue lines

Supplementary Material 4: Figure S4. Inhibitory effects of rebamipide on α-synuclein+MPP^+-induced down-regulation of nucleus NF-κB in BV2 microglia cellsand the mouse substantia nigra pars compacta 3 d after 1-methyl-4-phenyl-1, 2, 3, 6-tetrahydropyridineinjection. ***$p <$ 0.001 compared with the control group; # $p < 0.05$ compared with the α-synuclein+MPP^+ or MPTP -treated groups.

Supplementary Material 5: Figure S5. Effects of rebamipide on IL-1ß receptors in dopaminergic neurons of substantia nigra pars compacta. Effects of rebamipide on IL-1ß receptors and tyrosine hydroxylase-specific immunostaining in vivo

Acknowledgements

Acknowledgments This work was supported by a grant on the development of sustainable application for standard herbal resources (KSN1823320), by a grant on the development of innovative technologies for the future value of herbal medicine resources (KSN2511030), and development of an upcycling platform technology for food waste utilization (KSN2511040) from the Korea Institute of Oriental Medicine, and by a grant on the Pharmacokinetic interaction and mechanistic investigation using isobologram and multi-omics analysis of traditional Korean medicine and western medicine concomitant therapy for establishing therapeutic basis in the treatment of Alzheimer's disease (RS-2024-00352796) from the National Research Foundation of Korea and by a grant on the Industial Innovation Infrastructure (RS-2024-00434342) from Korea Institute for Advancement of Technology (KIAT), Republic of Korea. We sincerely thank Professor Ki Hyun Kim from the School of Pharmacy, Sungkyunkwan University, for his valuable support in providing access to the Schrödinger software, which greatly facilitated our molecular docking studies.

Authors' contributions

Author Contributions Dr. G Park and Dr. HS Lim conceived the idea and designed the experiments. Dr. HS Lim, Dr. G Park, Dr. J Park, Prof. W Lee, Prof. E Kim, Prof. H Yun, and Dr. SH Lee performed the experiments and data analysis. Dr. Park, Prof. Lee, Prof. Yun, Prof. W Lee, and Dr. Lim assisted in data interpretation and manuscript preparation, and wrote the entire manuscript. All authors commented on and approved the manuscript.

Funding

This work was supported by a grant on the development of sustainable application for standard herbal resources (KSN1823320), by a grant on the development of innovative technologies for the future value of herbal medicine resources (KSN2511030), and development of an upcycling platform technology for food waste utilization (KSN2511040) from the Korea Institute of Oriental Medicine, and by a grant on the Pharmacokinetic interaction and mechanistic investigation using isobologram and multi-omics analysis of traditional Korean medicine and western medicine concomitant therapy for establishing therapeutic basis in the treatment of Alzheimer's disease (RS-2024–00352796) from the National Research Foundation of Korea and by a grant on the Industial Innovation Infrastructure (RS-2024–00434342) from Korea Institute for Advancement of Technology (KIAT), Republic of Korea. We sincerely thank Professor Ki Hyun Kim from the School of Pharmacy, Sungkyunkwan University, for his valuable support in providing access to the Schrödinger software, which greatly facilitated our molecular docking studies.

Data availability

Data availability statement Data from the study is available from the corresponding author upon reasonable request.

Declarations

Ethics approval and consent to participate

All animal procedures were approved by the Animal Care and Use Committee of KIOM (Approval number: IACUC-KIOM-22–026, 22–075, and 23–060) and Macrogen, Inc. (Approval number: IACUC-MS-2023–01) and conducted in accordance with relevant guidelines and regulations.

Competing interests

The authors declare no competing interests.

Author details

[1]Herbal Medicine Resources Research Center, Korea Institute of Oriental Medicine, 111 Geonjae-Ro, Naju-Si, Jeollanam-Do 58245, Republic of Korea. [2]Department of Chemistry, Sungkyunkwan University, Suwon 16419, Republic of Korea. [3]Department of Biology, KNU G-LAMP Research Center, KNU Institute of Basic Sciences, BK21 FOUR KNU Creative BioResearch Group, College of Natural Sciences, Kyungpook National University, Daegu 41566, Republic of Korea. [4]Department of MetaBioHealth, SKKU Institute for Convergence, Sungkyunkwan University, Suwon 16419, Republic of Korea. [5]College of Pharmacy, Chungnam National University, Daejeon, Republic of Korea. [6]Convergence Research Center, Chungnam National University, Daejeon, Republic of Korea. [7]Department of Bio-AI Convergence, Chungnam National University, Daejeon, Republic of Korea. [8]Department of Biochemistry, Research Institute for Medical Science, Chungnam National University School of Medicine, 282 Munhwa-Ro, Jung-Gu, Daejeon 35015, Republic of Korea.

Received: 1 April 2025 Accepted: 4 May 2025
Published online: 17 May 2025

References

1. Jellinger KA. Parkinson's disease. In: Dickson DW, Weller RO, editors. Neurodegeneration: the molecular pathology of dementia and movement disorders. Oxford: Wiley-Blackwell; 2011. p. 194–223.
2. Ureshino RP, Ramírez AL. Linking aging and animal models to neurodegeneration: the striatum, substantia nigra, and Parkinson's disease. In: Assessments, Treatments and Modeling in Aging and Neurological Disease. Elsevier; 2021. p. 539–552
3. Kouli A, Spindler LR, Fryer TD, Hong YT, Malpetti M, Aigbirhio FI, et al. Neuroinflammation is linked to dementia risk in Parkinson's disease. Brain. 2024;147:923–35.
4. Huang S, Chen Z, Fan B, Chen Y, Zhou L, Jiang B, et al. A selective NLRP3 inflammasome inhibitor attenuates behavioral deficits and neuroinflammation in a mouse model of Parkinson's disease. J Neuroimmunol. 2021;354:577543.
5. Lee E, Hwang I, Park S, Hong S, Hwang B, Cho Y, et al. MPTP-driven NLRP3 inflammasome activation in microglia plays a central role in dopaminergic neurodegeneration. Cell Death Differ. 2019;26:213–28.
6. Haque ME, Akther M, Jakaria M, Kim IS, Azam S, Choi DK. Targeting the microglial NLRP3 inflammasome and its role in Parkinson's disease. Mov Disord. 2020;35:20–33.
7. Liu Q, Zhang M-M, Guo M-X, Zhang Q-P, Li N-Z, Cheng J, et al. Inhibition of microglial NLRP3 with MCC950 attenuates microglial morphology and NLRP3/caspase-1/IL-1β signaling in stress-induced mice. J Neuroimmune Pharmacol. 2022;17:503-14. https://pubmed.ncbi.nlm.nih.gov/34978026/
8. Naito Y, Yoshikawa T. Rebamipide: a gastrointestinal protective drug with pleiotropic activities. Expert Rev Gastroenterol Hepatol. 2010;4:261–70.
9. Liu J, Shen-Tu J, Wu L, Dou J, Xu Q, Zhou H, et al. Development of a simple LC-MS/MS method for determination of rebamipide in human plasma and its application to a bioequivalence study. Pharmazie. 2012;67:906–11.
10. Genta R. The role of Rebamipide in the management of inflammatory disease of the gastrointestinal tract. Aliment Pharmacol Ther. 2003;18:8–13.
11. Arakaki R, Eguchi H, Yamada A, Kudo Y, Iwasa A, Enkhmaa T, et al. Anti-inflammatory effects of rebamipide eyedrop administration on ocular lesions in a murine model of primary Sjögren's syndrome. PLoS ONE. 2014;9:e98390.
12. Kashima T, Itakura H, Akiyama H, Kishi S. Rebamipide ophthalmic suspension for the treatment of dry eye syndrome: a critical appraisal. Clin Ophthalmol. 2014;8:1003–10. https://pubmed.ncbi.nlm.nih.gov/24940041/.
13. Murakami I, Zhang R, Kubo M, Nagaoka K, Eguchi E, Ogino K. Rebamipide suppresses mite-induced asthmatic responses in NC/Nga mice. Am J Physiol Lung Cell Mol Physiol. 2015;309:L872–8.
14. Gendy AM, Abdallah DM, El-Abhar HS. The potential curative effect of rebamipide in hepatic ischemia/reperfusion injury. Naunyn Schmiedebergs Arch Pharmacol. 2017;390:691–700.
15. Moon SJ, Park JS, Woo YJ, Lim MA, Kim SM, Lee SY, et al. Rebamipide suppresses collagen-induced arthritis through reciprocal regulation of Th17/Treg cell differentiation and heme oxygenase 1 induction. Arthritis Rheumatol. 2014;66:874–85.
16. Li W, Zhao Y, Xu X, Ma W, Gao P, Wang Y, et al. Rebamipide suppresses TNF-α mediated inflammation *in vitro* and attenuates the severity of dermatitis in mice. FEBS J. 2015;282:2317–26.
17. Funahashi Y, Yoshida M, Yamamoto T, Majima T, Takai S, Gotoh M. Intravesical application of rebamipide suppresses bladder inflammation in a rat cystitis model. J Urol. 2014;191:1147–52.
18. Yoshida H, Hashimoto Y, Fukushima T, Tanji K, Matsumiya T, Seya K, et al. Effect of low-concentration amyloid-β 1–42 (Aβ42) on human neuroblastoma SH-SY5Y cell viability: neuroprotective potential of combination use with carnosic acid, rebamipide, edaravone, and resveratrol. Hirosaki Igaku. 2019;70:24–38.
19. Fukui K, Yachi K, Yoshida H, Tanji K, Matsumiya T, Hayakari R, et al. Rebamipide reduces amyloid-β 1–42 (Aβ42) production and ameliorates Aβ43-lowered cell viability in cultured SH-SY5Y human neuroblastoma cells. Neurosci Res. 2017;124:40–50.
20. Mishra A, Krishnamurthy S. Rebamipide mitigates impairments in mitochondrial function and bioenergetics with α-synuclein pathology in 6-OHDA-induced Hemiparkinson's model in rats. Neurotox Res. 2019;35:542–62.
21. Kim YS, Joh TH. Microglia, major player in the brain inflammation: their roles in the pathogenesis of Parkinson's disease. Exp Mol Med. 2006;38:333–47.
22. Lofrumento DD, Saponaro C, Cianciulli A, De Nuccio F, Mitolo V, Nicolardi G, et al. MPTP-induced neuroinflammation increases the expression of pro-inflammatory cytokines and their receptors in mouse brain. NeuroImmunoModulation. 2010;18:79–88.
23. Tang Y, Le W. Differential roles of M1 and M2 microglia in neurodegenerative diseases. Mol Neurobiol. 2016;53:1181–94.
24. Guo S, Wang H, Yin Y. Microglia polarization from M1 to M2 in neurodegenerative diseases. Front Aging Neurosci. 2022;14:815347.
25. Lim HS, Moon BC, Lee J, Choi G, Park G. The insect molting hormone 20-hydroxyecdysone protects dopaminergic neurons against MPTP-induced neurotoxicity in a mouse model of Parkinson's disease. Free Radic Biol Med. 2020;159:23–36.
26. Petzinger GM, Walsh JP, Akopian G, Hogg E, Abernathy A, Arevalo P, et al. Effects of treadmill exercise on dopaminergic transmission in the 1-methyl-4-phenyl-1,2,3,6-tetrahydropyridine-lesioned mouse model of basal ganglia injury. J Neurosci. 2007;27(20):5291–300.
27. Song GJ, Suk K. Pharmacological modulation of functional phenotypes of microglia in neurodegenerative diseases. Front Aging Neurosci. 2017;9:139.
28. Calvello R, Cianciulli A, Nicolardi G, De Nuccio F, Giannotti L, Salvatore R, et al. Vitamin D treatment attenuates neuroinflammation and dopaminergic neurodegeneration in an animal model of Parkinson's disease, shifting M1 to M2 microglia responses. J Neuroimmune Pharmacol. 2017;12:327–39.
29. Bové J, Perier C. Neurotoxin-based models of Parkinson's disease. Neuroscience. 2012;211:51–76.
30. Zhang Q-S, Heng Y, Yuan Y-H, Chen N-H. Pathological α-synuclein exacerbates the progression of Parkinson's disease through microglial activation. Toxicol Lett. 2017;265:30–7.
31. Sanchez-Guajardo V, Barnum CJ, Tansey MG, Romero-Ramos M. Neuroimmunological processes in Parkinson's disease and their relation to α-synuclein: microglia as the referee between neuronal processes and peripheral immunity. ASN Neuro. 2013;5:AN20120066.
32. Feng Y, Li M, Yangzhong X, Zhang X, Zu A, Hou Y, et al. Pyroptosis in inflammation-related respiratory disease. J Physiol Biochem. 2022;78:721–37.

33. Wu C, Zhou L, Yuan H, Wu S. Interconnections among major forms of regulated cell death. Apoptosis. 2020;25:616–24.
34. Panicker N, Kam T-I, Wang H, Neifert S, Chou S-C, Kumar M, et al. Neuronal NLRP3 is a parkin substrate that drives neurodegeneration in Parkinson's disease. Neuron. 2022;110:2422-37.e2429.
35. Duan M, Sun L, He X, Wang Z, Hou Y, Zhao Y. Medicinal chemistry strategies targeting NLRP3 inflammasome pathway: A recent update from 2019 to mid-2023. Eur J Med Chem. 2023;260:115750.
36. Yao S, Li L, Sun X, Hua J, Zhang K, Hao L, et al. FTY720 inhibits MPP+-induced microglial activation by affecting NLRP3 inflammasome activation. J Neuroimmune Pharmacol. 2019;14:478–92.
37. Kim J, Ahn H, Yu S, Ahn J-H, Ko H-J, Kweon M-N, et al. IκBζ controls NLRP3 inflammasome activation via upregulation of the Nlrp3 gene. Cytokine. 2020;127:154983.
38. Fu J, Wu H. Structural mechanisms of NLRP3 inflammasome assembly and activation. Annu Rev Immunol. 2023;41:301–16.
39. Abbott NJ. Blood–brain barrier structure and function and the challenges for CNS drug delivery. J Inherit Metab Dis. 2013;36:437–49.
40. Mateev E, Kondeva-Burdina M, Georgieva M, Zlatkov A. Repurposing of FDA-approved drugs as dual-acting MAO-B and AChE inhibitors against Alzheimer's disease: An in silico and *in vitro* study. J Mol Graph Model. 2023;122:108471.

Publisher's Note